Cheng, A., Hummel, B., Mencke, A. & Caffrey, M. Kinetics and mechanism of the barotropic lameller gel/lameller liquid crystal phase transition in fully hydrated dihexadecylphosphat...

4 AUTHORS, INCLUDING:

Andrés P Mencke

V. I. Research

9 PUBLICATIONS **117** CITATIONS

Kinetics and Mechanism of the Barotropic Lamellar Gel/Lamellar Liquid Crystal Phase Transition in Fully Hydrated Dihexadecylphosphatidylethanolamine: A Time-Resolved X-Ray Diffraction Study Using Pressure Jump

Anchi Cheng, Bernard Hummel, Andrés Mencke, Martin Caffrey
Department of Chemistry, The Ohio State University Columbus, Ohio 43210 USA

ABSTRACT   The kinetics and mechanism of the barotropic lamellar gel ($L_{\beta'}$)/lamellar liquid crystal (L_α) phase transition in fully hydrated 1,2-dihexadecyl-sn-glycero-3-phosphoethanolamine (DHPE) has been studied using time-resolved x-ray diffraction (TRXRD). The phase transition was induced by pressure jumps of varying amplitudes in both the pressurization and depressurization directions at controlled temperature (78°C). Both low- and wide-angle diffracted x rays were recorded simultaneously in live time using an x-ray-sensitive image intensifier coupled to a CCD camera and Super-VHS videotape recorder. Such an arrangement allowed for the direct and quantitative characterization of the long- (lamellar repeat spacing) and short-range order (chain packing) during a kinetic experiment. The image-processed live-time x-ray diffraction data were fitted using a nonlinear least-squares model, and the parameters of the fits were monitored continuously throughout the transition. The pressure-induced transitions from the L_α to the $L_{\beta'}$ phase and from the $L_{\beta'}$ to the L_α phase was two-state (no formation of intermediates apparent during the transition) to within the sensitivity limits of the method. The corresponding transit time (the time during which both phases coexist) associated with the long- and short-range order of the pressurization-induced L_α-to-$L_{\beta'}$ phase transition decreased to a limiting value of approximately 50 ms with increasing pressure jump amplitude. This limiting value was close to the response time of the detector/recording system. Thus, the intrinsic transit time of this transition in fully hydrated DHPE at 78°C was less than or equal to 50 ms. In contrast, the depressurization-induced $L_{\beta'}$-to-L_α phase transition was slower, taking approximately 1 s to complete, and occurred with no obvious dependence of the transit time on pressure jump amplitude. In the depressurization jump experiment, the lipid responded rapidly to the pressure jump in the $L_{\beta'}$ phase up to the rate-determining $L_{\beta'}$-to-L_α transition. Such behavior was examined carefully, as it could complicate the interpretation of phase transition kinetic measurements.

INTRODUCTION

Thermodynamic variables such as pressure and temperature have been used to trigger phase transitions in studies of the dynamics and mechanism of lipid mesophase interconversions (see Caffrey, 1989; Gruner, 1987; Laggner and Kriechbaum, 1991; Marsh, 1991; and Van Osdol et al., 1989 for recent reviews). In relaxation kinetic measurements, the pressure jump trigger has been shown to offer several advantages over the temperature jump approach (Mencke and Caffrey, 1991; Yager and Peticolas, 1982). A study of the kinetics and mechanism of the lamellar gel ($L_{\beta'}$)/lamellar liquid crystal (L_α) phase transition in fully hydrated 1,2-dihexadecyl-sn-glycero-3-phosphoethanolamine (DHPE) induced by pressure has been reported previously (Mencke and Caffrey, 1991). Structural details of the transition itself were monitored by time-resolved x-ray diffraction (TRXRD), and the pressure jumps were implemented by manually opening valves either to a compressed air cylinder or to atmosphere. In these measurements the pressure jump itself lasted 2 s, and the amplitude of the jump was limited to 9.6 MPa. In the present study we have examined the same transition in the same hydrated lipid but with a much-improved pressure apparatus with which rapid (<10 ms) and variable large-amplitude (up to 131 MPa) pressure jumps were possible.

The results of the present study show that the kinetics of the $L_{\beta'}$/L_α phase change are quite different depending on the direction from which the transition is approached. Further, we have observed immediate and rapid shifts in the position of the lamellar and the chain-packing reflections of the $L_{\beta'}$ phase during the course of the depressurization jump measurements. The response is ascribed to an initial, fast decompression of the $L_{\beta'}$ phase, which brings the system to the point where the rate-limiting $L_{\beta'}$-to-L_α phase conversion takes place.

Abbreviations used: b(x), background as a function of radial distance; DHPE, 1,2-dihexadecyl-sn-glycero-3-phosphoethanolamine; H_{II}, inverted hexagonal phase; L_α, lamellar liquid crystal phase; $L_{\beta'}$, lamellar gel phase; SOPE, 1-stearoyl-2-oleoyl-sn-glycero-3-phosphoethanolamine; TRXRD, time-resolved x-ray diffraction. Units of pressure: 1 atm = 1.013×10^6 dynes/cm² = 1.013 bars = 1.013×10^5 N·m⁻² = 0.1013 MPa = 14.696 psi = 76 cm Hg (at 0°C) = 760 torr (at 0°C).

MATERIALS AND METHODS

Materials

DHPE was obtained from Serdary Research Laboratories (London, Ontario, Canada) and was used without further purification. Water used in sample preparation was obtained from a Milli-Q purification system (Millipore

Corp., Bedford, MA) and tap water was used in the pressure apparatus as the pressure-transmitting medium. The latter was prevented from contacting the sample directly by means of a Parafilm plug (Mencke et al., 1993) separating the sample from the rest of the pressure apparatus. All other chemicals used were of reagent grade.

Sample preparation

DHPE samples in excess water were prepared by placing ~100 mg of pure lipid and 100–125 mg water into a mixing device consisting of two syringes connected end-to-end through a small-orifice coupler (Cheng et al., manuscript in preparation). Mixing was performed by increasing the temperature of the sample in the mixer to above its $L_{\beta'}$-to-L_{α} transition at 68.5°C (Seddon et al., 1983) and forcing the sample and water back and forth 200 to 300 times through the coupler, effecting mechanical mixing of the sample. The sample was then transferred from the mixer to the beryllium pressure cell via a long 22-gauge syringe needle.

TRXRD

The TRXRD measurements were made using the A1 line at the Cornell High Energy Synchrotron Source (Fig. 1) as described previously (Caffrey, 1987; Mencke and Caffrey, 1991). The wiggler-enhanced white radiation was both monochromatized and horizontally focused using a 10-cm long cylindrically

bent, asymmetric, triangular germanium (111) crystal. The beam was then vertically focused and higher harmonics were eliminated by a 60 cm-long nickel-coated mirror. The x-ray beam entered the experimental hutch through adjustable horizontal and vertical slits and was collimated using a 0.3 mm collimator (Charles Supper Co., Natick, MA).

Both low- and wide-angle diffracted x rays were imaged on the TRXRD detection system as described previously (Caffrey et al., 1991). Such an arrangement allowed for the direct determination and characterization of the long- and short-range order within the sample simultaneously during a kinetic experiment. A character generator was used to encode elapsed time, experiment number, and pressure directly onto the video signal so that they were recorded simultaneously with the 2D diffraction pattern.

The intrinsic rise and decay times for the TRXRD detection system were measured as described previously (Caffrey, 1985) with a time resolution of one video field (1/60 s, 17 ms). To this end, the x-ray shutter was opened and closed while a strong lipid diffraction pattern was being recorded in live time on videotape. The change in the area of a single diffraction peak (I-2θ, see below) recorded in this manner was then analyzed using image processing and nonlinear fitting, as described below. The increase in peak area with time upon opening the x-ray shutter was roughly exponential (of the form 1-exp(-t), where t is time). Such measurements yielded a 10 to 90% rise time of 50–70 ms. The decay curve could be resolved into three components: 1), a fast-decaying component that accounted for a reduction to 20% of the original intensity value in the first 30 ms; 2), a component of intermediate decay rate that reduced the peak area to 10% of the original
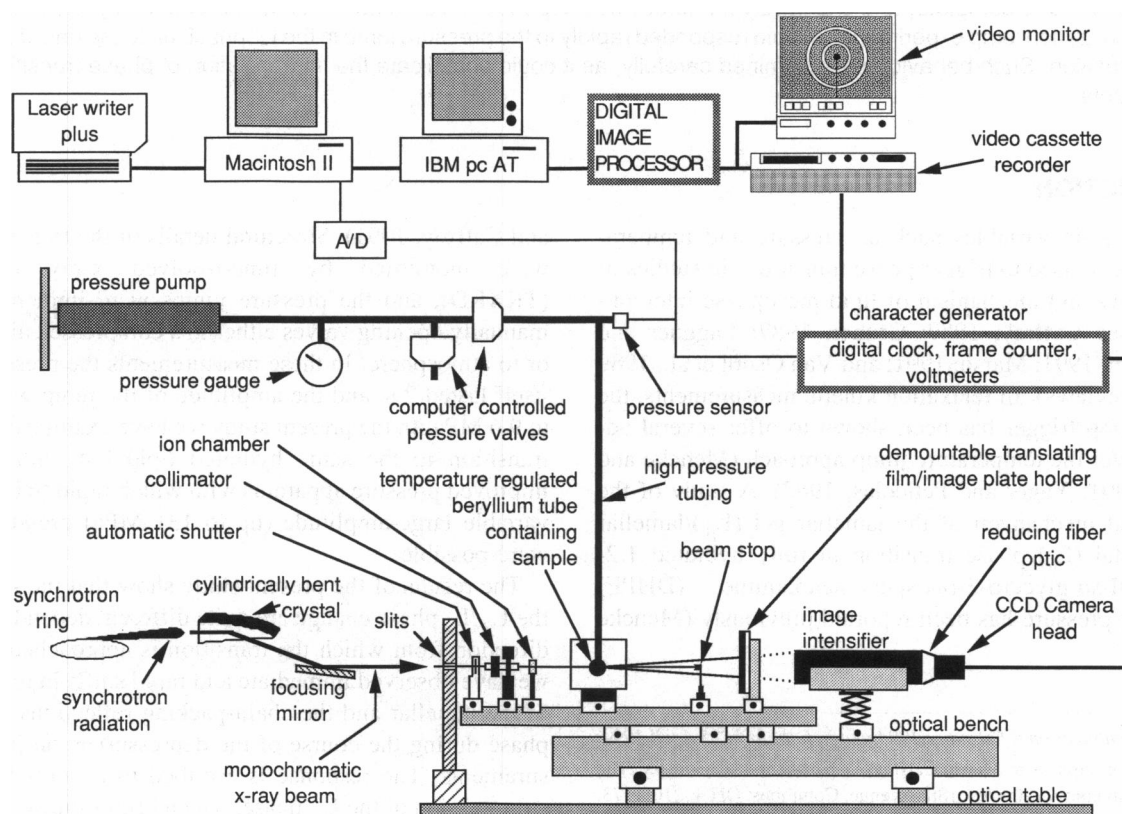

FIGURE 1   Schematic diagram of the experimental arrangement for monitoring x-ray diffraction in live time using synchrotron radiation (not drawn to scale). White radiation from the synchrotron is simultaneously monochromatized ($\lambda = 1.555$ Å) and horizontally focused by a 10 cm-long, cylindrically bent germanium crystal. Higher-order harmonic contaminants are eliminated and the 8-keV beam reflected and vertically focused by a 60-cm long nickel-coated mirror. The monochromatic beam is passed through a 0.3-mm collimator. Both low- and wide-angle diffracted x rays are allowed to strike the fluorescent screen on the front face of a three-stage intensifier tube used for image intensification. The distance between the sample and the front face of the image intensifier is 32 mm. The image is displayed dynamically on the intensifier tube and recorded in live time using a fiberoptically coupled CCD camera and an S-VHS video cassette recorder. The lipid sample is contained in an x-ray "transparent" beryllium cell specifically designed for these pressure experiments. Along with the two-dimensional diffraction image, the pressure, experiment number, elapsed time in seconds, and video frame number are recorded simultaneously on videotape. Data analysis is performed using a digital image processor under computer control.

during the next 100 ms; and 3), a slowly decaying component that gave rise to a faint "ghost" diffraction pattern (~3% intensity) 1 s after closing the shutter.

X-radiation damage to the sample was kept to a minimum by implementing procedures described previously (Caffrey, 1984). The x-ray wavelength (1.555 Å) was determined by using a lead nitrate standard and a carefully measured sample-to-film distance (Caffrey, 1987).

Pressure apparatus

The pressure apparatus used in making the measurements has been described previously (Mencke et al., 1993). The essential features of the setup are illustrated in Fig. 1. Sample temperature was held at 78°C by using a temperature controller (type 812, Eurotherm, Reston, VA) and a forced-air heater directed over the beryllium sample cell. The temperature was monitored by a thermocouple positioned next to where the x-ray beam struck the sample cell.

In the case of one set of depressurization jump measurements in the $L_{\beta'}$ phase, the temperature was maintained at 75°C using a thermostated copper block and a circulating water bath as described previously (Mencke et al., 1993). The in-sample temperature was monitored during this experiment as described previously (Mencke et al., 1993) and the computer-recorded temperature was reported. The precision of the temperature measurement was ±0.1°C with an accuracy of ±1.0°C.

Pressure jumps were initiated as described previously (Mencke et al., 1993). Pressure jumps in both directions and over the full range of amplitudes used had a response time (from 10 to 90% of the pressure jump amplitude) of less than 10 ms. The pressure recorded was that sensed by a diaphragm strain gauge (model HP/56510–2, Sensotec Inc., Columbus, OH) located near the sample cell (Fig. 1) so that it accurately reflected the time course of the pressure jump inside the sample cell. The pressure-dependent output of the gauge was recorded on both videotape and computer. The accuracy of the pressure reading was ±3 MPa.

Data analysis

TRXRD data were analyzed by previously described methods (Mencke and Caffrey, 1991) with the following parameters and modifications. Successive frames of the live-time x-ray diffraction patterns recorded on Super-VHS videotape (30 frames/s) were digitized using a digital image processing technique (hardware Trapix 55/48, Recognition Concepts Inc., Carson City, NV; software RTIPS, Tau Corp., Los Gatos, CA, and homewritten software). In some cases, the first few video frames of the transition were separated further into fields to facilitate analysis of the data with higher time resolution (1/60 s) during the period of most rapid change. However, all data shown in the figures below was derived from frames rather than fields. The images were radially averaged over a 20° arc, centered on the vertical axis of the diffraction pattern, to produce an intensity (I) versus position (scattering angle, 2θ) plot for each image. The data were then ported to a Macintosh II computer where each I-2θ scan was fitted using a nonlinear least-squares method to a model function consisting of between one and three Lorenzian functions and a background as follows:

$$f_{fit}(x, M_1, \mu_1, \sigma_1, M_2, \mu_2, \sigma_2, M_3, \mu_3, \sigma_3, C)$$

$$= \frac{M_1}{1 + \left(\dfrac{x - \mu_1}{\sigma_1}\right)^2} + \frac{M_2}{1 + \left(\dfrac{x - \mu_2}{\sigma_2}\right)^2} + \frac{M_3}{1 + \left(\dfrac{x - \mu_3}{\sigma_3}\right)^2} + b(x) + C \qquad (1)$$

where x is the radial distance from the center of the powder diffraction pattern, $b(x)$ is a fixed Lorenzian background function used to describe the background scattering profile beneath the diffraction peaks, C is a constant providing for the fine adjustment of $b(x)$ to each image, and M, μ, and σ are the peak height, radial position and the half-width-at-half-height, respectively. The subscript index numbers refer to as many as three observed diffraction peaks seen at any one time during the course of an experiment. The fit parameters (M, μ, σ), and calculated peak area ($\pi M \sigma$) of the diffraction peaks were determined as a function of time throughout the tran-

sition. The calculated area of the different phases was used to monitor the progress of the phase transition. This is based on the assumption that peak area is proportional to the amount of material giving rise to the diffraction peak at a fixed scattering angle (Klug and Alexander, 1974).

Transit time is defined as the time interval between the first sighting of diffraction from the newly forming phase and the last detectable diffraction from the phase undergoing transformation and is estimated by visual examination of the recorded data on the video screen and from the progress curves. The lower bound to the measurable transit time is ~50 ms and is limited by the intrinsic rise and decay time of the detection/recording system. Except for radial averaging, the data presented in the I-2θ plots below correspond to the raw, uncorrected data.

RESULTS

To facilitate a description of the experimental measurements and an evaluation of the results, a schematic pressure-temperature phase diagram of hydrated DHPE is shown in Fig. 2. It is based on equilibrium measurements that will be reported separately (Cheng et al., manuscript in preparation). In this figure we see that at any pressure, the $L_{\beta'}$ phase is the low-temperature phase that transforms into the L_α phase upon heating. Further, the $L_{\beta'}/L_\alpha$ transition temperature is 68.5°C at atmospheric pressure, and the transition temperature rises by 0.251°C for every 1-MPa increase in pressure (Cheng et al., 1992). Because the specific volume of the $L_{\beta'}$ phase is less than that of the L_α phase (Tardieu et al., 1973), the former represents the high-pressure phase. Therefore, the L_α-to-$L_{\beta'}$ transition can be induced by increasing pressure and/or reducing temperature.

Pressurization jump measurements of the L_α-to-$L_{\beta'}$ phase transition

During the course of the pressurization jump measurements, the barotropic L_α-to-$L_{\beta'}$ transition was found to be rapid and
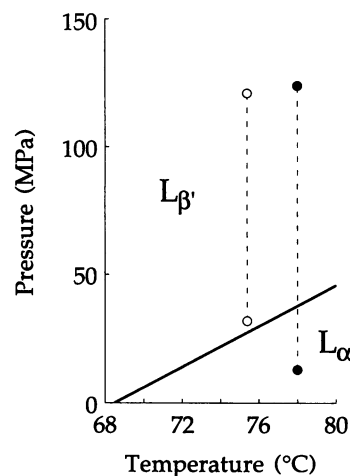

FIGURE 2   Schematic pressure-temperature phase diagram of fully hydrated DHPE. The slope of the $L_\alpha/L_{\beta'}$ phase boundary is 3.98 MPa/°C (Cheng et al., 1992). The transition temperature of 68.5°C at ambient pressure was measured by differential scanning calorimetry. *Circles* connected by *dashed lines* are included to show temperatures at and pressures to and from which pressure jump measurements were made. These involved the $L_{\beta'}$-to-L_α transition (●) described in Figs. 4 and 5 and the $L_{\beta'}$ phase alone (○) described in Fig. 6. See text for details.

two-state (Table 1, Fig. 3). No intermediates were detected in either the low- or wide-angle region of the time-resolved diffraction patterns (corresponding to the lamellar repeat and the chain packing spacing, respectively) to within the sensitivity limits of the recording/analysis system. The transit times measured showed a pronounced dependence on pressure jump amplitude (Table 1). Thus, as the amplitude increased, the transit time decreased to a limiting value of ~50 ms. This value corresponds to the rise and initial decay time of the x-ray detection/recording system (see Materials and Methods). Thus, the intrinsic transit time for the pressure-induced L_α-to-$L_{\beta'}$ phase transition can be set at $\leq$50 ms.

Although the L_α-to-$L_{\beta'}$ transition itself was fast, a slower relaxation of the newly formed $L_{\beta'}$ phase was observed after the transition was completed. This was most apparent in the peak height and radial position progress curves recorded in both low- and wide-angle regions of the diffraction pattern (Fig. 3). The relaxation times of these relatively slow, post-transition processes for the different pressurization jump experiments were of order 1–2 s and did not show a dependence on pressure jump amplitude (data not shown).

Depressurization jump measurements of the $L_{\beta'}$-to-L_α phase transition

The kinetics of the depressurization jump experiments wherein the $L_{\beta'}$-to-L_α phase transition was induced were markedly different from those of the pressurization jump measurements (above) despite the observation that both were of the two-state type. The depressurization transition was considerably slower and was of ~1 s duration with no noticeable dependence on pressure jump amplitude (Table 1).

The wide-angle data collected in the depressurization jump experiments revealed the presence of a new reflection in the course of the measurement, which gave rise to some difficulty in interpreting the transition mechanism. Thus, immediately after the depressurization jump perturbation, a sharp diffraction ring (hereafter referred to as RII) appeared to the low-angle side of the original gel chain packing reflection (hereafter referred to as RI) (Figs. 4 and 5 B). With time, RII, along with the residual RI signal (resulting from the intrinsic decay of the detection system described in Materials and Methods) declined and gave way to a growing diffuse scatter from the disordered chains of the L_α phase (Figs. 4 and 5). As the amplitude of the pressure jump increased, the diffraction angle of RI increased, whereas that of RII remained constant. Thus, the two reflections were farther apart and more discernible as distinct peaks at larger pressure jump amplitudes. Interestingly, a corresponding new reflection in the low-angle region was not observed during the lifetime of RII. However, a small but consistent increase in the radius of the $L_{\beta'}$ (004) reflection was found in the depressurization jumps of larger amplitudes. In a separate experiment performed under the same conditions but with improved spatial resolution obtained by recording only the (001) reflection, a depressurization jump like the one shown in Figs. 4 and 5 caused a reduction in the lamellar repeat spacing of the $L_{\beta'}$ phase by 0.7 Å (data not shown). These results are considered more fully under Discussion.

Within a given pressure jump experiment, the chain order/disorder transition, as recorded in the wide-angle region of the diffraction pattern, began before or simultaneously with but never after the transition as observed in the low-angle region (Table 1). The time difference between the beginning of the transition as detected simultaneously in the low- and wide-angle regions, however, was reduced for the pressurization (L_α-to-$L_{\beta'}$) compared with the depressurization ($L_{\beta'}$-to-L_α) experiments. Peculiar to the depressurization jump experiments is the fact that the larger the pressure jump

---

TABLE 1   Transit time of the barotropic phase transition undergone by hydrated DHPE in response to a pressure jump*

	Pressure Jump			Transit Time[‡]		
Direction	Initial → Final	Amplitude		Low-Angle (004)	Wide-Angle	Δt_{onset}[§]
	MPa	MPa		s	s	s
Pressurization ($L_\alpha \rightarrow L_{\beta'}$)	26 → 68	42		0.31	0.33	0.00
	26 → 70	44		0.22	0.15	0.00
	26 → 94	68		0.08	0.07	0.04
	26 → 116	90		0.05	0.05	0.03
	29 → 140	111		0.05	0.07	0.00
	10 → 125	115		0.05	0.07	0.02
Depressurization ($L_{\beta'} \rightarrow L_\alpha$)	71 → 13	58		0.72	0.89	0.00
	96 → 13	83		0.97	0.81	0.03
	119 → 13	106		0.67	0.88	0.80
	124 → 13	111		1.08	0.95	0.15
	144 → 13	131		0.90	1.01	0.20

* Progress of the transition was monitored by simultaneous low- and wide-angle time-resolved x-ray diffraction.

[‡] Transit time refers to the time it takes to undergo the phase transition as judged by visual inspection of the video-recorded time-resolved x-ray diffraction images of the indicated reflections and progress curves of the fitted diffraction profiles. Transit time is defined as the time interval between the first sighting of the newly forming phase and last detectable diffraction from the phase undergoing the transformation. The shortest measurable transit time is 0.05 s, which is determined by the intrinsic rise and decay time of the detection/recording system.

[§] Δt_{onset} is the difference in time between the onset of the phase transition observed in the wide- and low-angle diffraction region.

FIGURE 3   Kinetics of the L_α-to-$L_{\beta'}$ phase transition in fully hydrated DHPE in response to a 29- to 140-MPa pressure jump. Low-angle (the fourth order lamellar reflection [004]) (A) and wide-angle (B) diffracted x rays were recorded simultaneously in live time, and the area (I), peak height (II), radial position (III), and half-width-at-half-peak-height (IV) were obtained by image processing and least-squares fitting using Eq. 1. Each data point in the figure corresponds to a single video frame (33 ms) with radial averaging over a 20° arc. The sample was maintained at a constant temperature of 78°C, and sample pressure was encoded on the video signal by means of a pressure sensor coupled to a character generator (Fig. 1). The pressure change with time during the course of the experiment is shown in (V). We have not established the origin of the small (<5% of the pressure jump amplitude) and gradual pressure rises which began <200 ms before the main pressure jump event. Inspection of these data indicate that the transit times associated with the low- and wide-angle diffraction measurements are 0.05 and 0.07 s, respectively (Table 1).
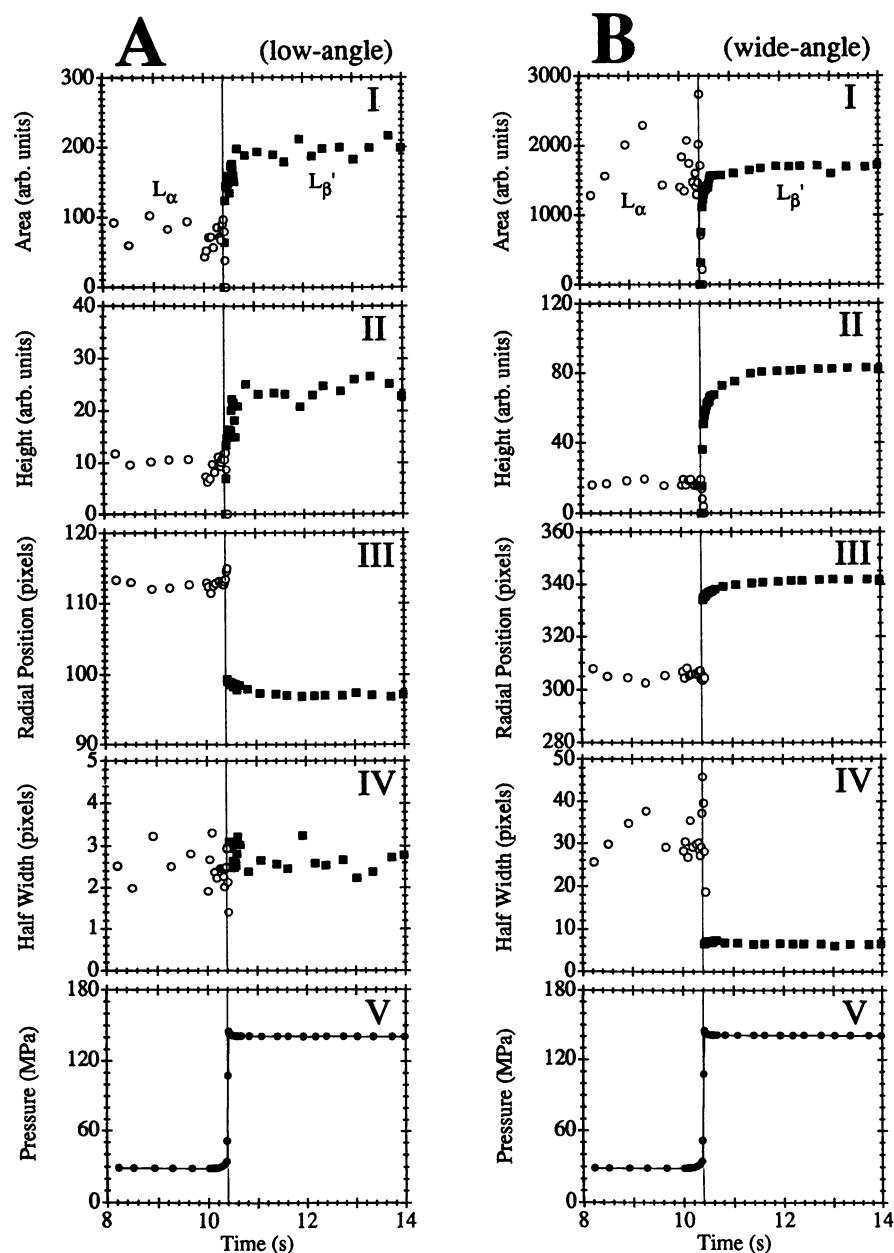
amplitude, the longer was the time delay between the beginning of the changes in the low- and wide-angle regions.

Depressurization jump measurements in the $L_{\beta'}$ phase

By way of understanding the origin of the enigmatic RII reflection described in the preceding section, the response of fully hydrated DHPE in the $L_{\beta'}$ phase to a pressure jump was examined. The jump was effected from 121 to 32 MPa at 75.4°C (Fig. 2). At this temperature, the $L_{\beta'}/L_\alpha$ transition pressure is 27.6 MPa (Cheng et al., 1992). Thus, the pressure jump took place entirely within the $L_{\beta'}$ phase. Before carrying out the experiment, the wide-angle region of the dif-

fraction pattern from the compressed lipid at 121 MPa showed the characteristic sharp reflection (RI) in the vicinity of 4.2 Å. Immediately upon release of pressure to 32 MPa, a reflection to the low-angle side of RI appeared. The latter corresponds to the RII reflection mentioned above. Its intensity grew at the expense of that associated with RI with a 10–90% rise time of 80 ms, a value close to the signal rise time of the detection/recording system. A slower relaxation which lasted ~1.5 s was also seen in the corresponding progress curves. The latter was most noticeable in the height and radial position curves (Fig. 6). Given that the depressurization perturbation should not induce a phase transition, no L_α phase was expected to form in the course of the measurement and indeed, none was found.
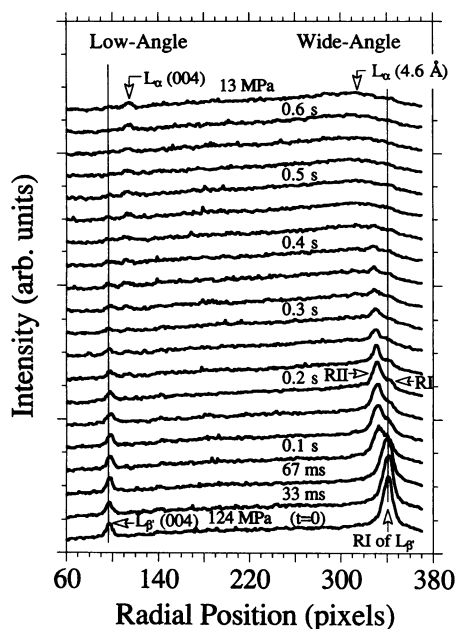
FIGURE 4 Stacked plot of intensity-versus-radial position for the $L_{\beta'}$-to-L_α phase transition undergone by fully hydrated DHPE in response to a 124–13 MPa pressure jump at 78°C. Each curve corresponds to a single video frame (33 ms) with radial averaging over a 20° arc. Successive frames are shown corresponding to a total time interval of 0.63 s (19 frames $\times$ 33 ms/frame). Before initiating the depressurization jump, the compressed $L_{\beta'}$ phase is evidenced by the presence of sharp reflections in the low-angle ([004] reflection at radial position = 98 pixel) and the wide-angle (pixel position 341, peak labeled RI) region. Immediately upon pressure release, which happens between the third and fourth frames in the stacked plot, a sharp reflection labeled RII is seen at a radial pixel position of 331 in the wide-angle region. This corresponds to the uncompressed form of the $L_{\beta'}$ phase. RII fades as the L_α phase develops, evidenced by the appearance of a sharp low-angle reflection at a radial position of 112 pixels and a broad wide-angle scattering peak centered at a radial pixel position of 311. The residual intensity associated with RI after the pressure release arises from the slowly decaying component of the detection/recording system (see text for details). The shift in position of the $L_{\beta'}$ low-angle [004] reflection to wider angle upon depressurization is barely visible (see text for details). Curves are displaced along the ordinate for clarity.

Simultaneously with the diffraction measurements, in-sample temperature was recorded during the course of the depressurization jump experiment (Fig. 6 VI). On the time scale of the pressure jump (< 10 ms), the system was essentially adiabatic. Thus, the pressure jump-related decompression was accompanied by a transient drop in sample temperature. However, because the system was not truly adiabatic, the original sample temperature was restored at a rate that reflects the heat transfer and heat capacity properties of the materials that make up the sample, the cell, and the surrounding environment. It is interesting to note that the rate at which the sample returned to its original temperature after the depressurization jump parallels the relaxation of the position of the decompressed $L_{\beta'}$ gel phase reflection (Fig. 6 VI). These important observations will be discussed more fully in the following section.

DISCUSSION

### Kinetics of the $L_{\beta'}/L_\alpha$ phase transitions

As noted above, the transit time of the pressure-driven L_α-to-$L_{\beta'}$ phase change shortens as the pressure jump amplitude increases. The transition was found to be at least as fast as could be measured considering the intrinsic response time of the detection/recording system for the larger pressure jumps used (Table 1). The L_α-to-$L_{\beta'}$ phase transition was also two-state, with no evidence for the formation of intermediates, to within the sensitivity limits of the detection, recording, and data analysis systems. This result agrees with related pressure jump measurements performed on the same system (Mencke and Caffrey, 1991).

The results of the depressurization jump experiments, however, were quite in contrast to those for the pressurization jump experiments. The transit times measured (approximately 1 s), based on both the low- and wide-angle data, were at least an order of magnitude larger and did not show a dependence on pressure jump amplitude. Because the $L_{\beta'}$-to-L_α phase transition requires the uptake of four molecules of water for every lipid molecule at atmospheric pressure (Hogan, 1989), the transit time for this water-imbibing phase transition may be limited by water transport (Caffrey, 1987; Mencke and Caffrey, 1991). In contrast, water loss during the pressurization jump may be faster because of the active nature of the process as well as the unique thermomechanical and transport properties of the transforming L_α phase (Mencke and Caffrey, 1991). Such a proposal might be tested by measuring transit times under water-stressed conditions. Nonetheless, we believe the values reported here represent the intrinsic transit times for the barotropic $L_{\beta'}$-to-L_α phase transition in fully hydrated DHPE at 78°C.

For purposes of comparison, we note that the transit time for the depressurization-induced $L_{\beta'}$-to-L_α transition recorded at 68°C in fully hydrated DHPE was 37 s (Mencke and Caffrey, 1991). In this experiment, the pressure jump amplitude used was 9.6 MPa, and the pressure jump itself lasted a full 2 s. This transit time is 30 to 40 times the value found in the present study. To what can we ascribe the difference? It is possibly a result of the faster water transport rate expected at the higher temperature (78°C vs. 68°C) (Caffrey, 1985) and/or the faster (<10 ms vs. 2 s) and larger-amplitude ($\geq$42 MPa vs. 9.6 MPa) pressure jumps used in this study in comparison with the previous one. Further systematic studies will be needed to establish firmly the origin of this disparate behavior.

We found no marked differences in the transit times of the simultaneously collected low- and wide-angle diffraction (Table 1). It was noticed, however, that in both pressurization and depressurization jump series, the start of the chain order/disorder transition, as observed in the wide-angle diffraction region, occurred before or simultaneously with, but never after the start of the transition observed in the low-angle

FIGURE 5 Kinetics of the $L_{\beta'}$-to-L_α phase transition in fully hydrated DHPE in response to a 124–13 MPa pressure jump at 78°C. Low-angle (the fourth order lamellar reflection [004]) (A) and wide-angle (B) diffracted x rays were recorded in live time and the area (I), peak height (II), radial position (III), and half-width-at-half-peak height (IV) was obtained by image processing. The pressure change with time is shown in (V). Other conditions are as described in the legend to Fig. 3. The transit times determined based on the low- and wide-angle diffraction data are 1.08 and 0.95 s, respectively (Table 1). The decay curve of peak area associated with RI after the pressure release (B, I) matches that of the detection/recording system.
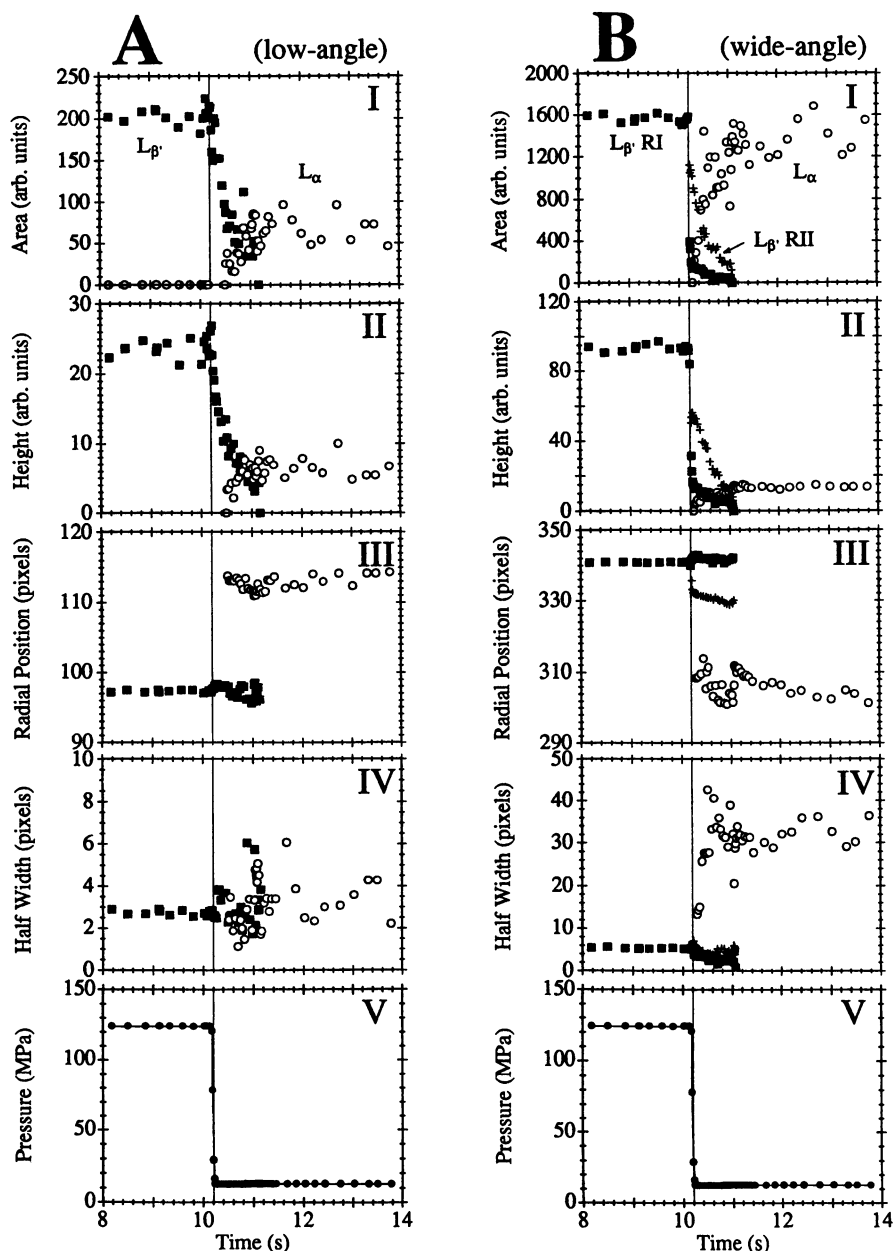
region (Table 1). The difference may indicate that further hydration of the lipid headgroup cannot proceed without chain melting.

In-phase structure relaxation

The wide-angle diffraction data collected during the course of the depressurization $L_{\beta'}$-to-L_α phase change revealed the presence of a new sharp reflection, identified as RII, to the low-angle side of the gel chain packing reflection (RI), which developed immediately after the release of pressure (Figs. 4 and 5 B). Concomitantly, the peak position of the lamellar (004) reflection shifted to higher scattering angles. These results are rationalized as follows (Fig. 7):

Previous diffraction studies have shown that the lamellar phase lattice dimensions are sensitive to pressure (Caffrey et al., 1991; Cheng et al., 1992; Winter et al., 1989). Thus, for example, upon application of pressure the rigid acyl chains of the $L_{\beta'}$ phase compress, which gives rise to a smaller chain packing and a larger lamellar repeat spacing (Cheng et al., 1992; Winter et al., 1989). Accordingly, when pressure is released, these structure changes are expected to reverse themselves so that the chain packing d-spacing increases and the lamellar repeat decreases. If the lipid dispersion, originally in the $L_{\beta'}$ phase under pressure, remains totally or partially in the $L_{\beta'}$ during decompression, the $L_{\beta'}$ phase diffraction pattern from such a system would be expected to show 1) a shift in the original wide-angle reflection
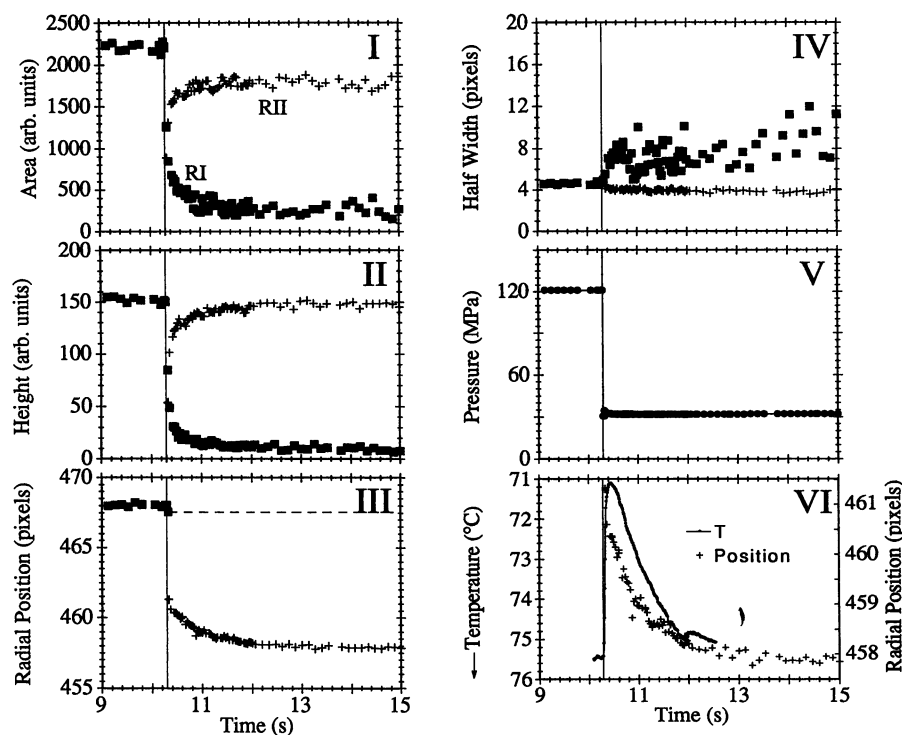
FIGURE 6   Kinetics of the $L_{\beta'}$ phase decompression in fully hydrated DHPE following a 121-to-32 MPa pressure jump at 75.4°C. Only wide-angle diffracted x rays were recorded in live-time in this experiment, and the area (*I*), peak height (*II*), radial position (*III*) and half-width-at-half-peak height (*IV*) were obtained by image processing. A fixed-peak position associated with the RI reflection after the pressure jump was used in the analysis and is shown in (*III*) as a horizontal dashed line. This is justified, as it is known that the residual intensity associated with the RI reflection observed after the jump is attributable to the slowly decaying component of the detection/recording system (see text for details). Each data point in the figure corresponds to a single (33 ms) frame with radial averaging over a 10° arc. Since the sample-to-detector distance in this measurement is different from that in Figs. 3, 4, and 5, the absolute value of the radial position in these figures cannot be compared directly. The pressure change with time during the course of the experiment is shown in (*V*). (*VI*) shows an expanded view of the data in panel III, which refers to the change in the position of RII with time superimposed on the in-sample temperature profile whose axis is shown increasing from top to bottom for easy comparison. In-sample temperature was recorded on a computer over a period of 2.5 s with a sampling interval of 10 ms.
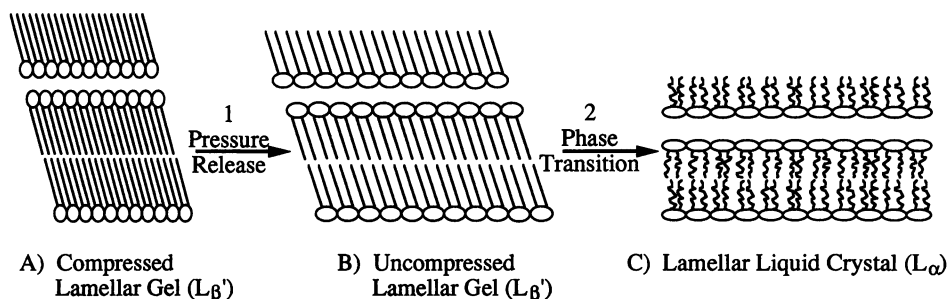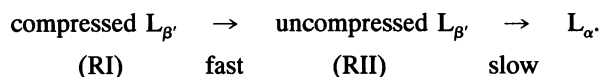

A) Compressed   B) Uncompressed   C) Lamellar Liquid Crystal (L_α)
   Lamellar Gel (L_β')   Lamellar Gel (L_β')

FIGURE 7   Proposed mechanism for the response of fully hydrated DHPE to a large depressurization jump through the $L_{\beta'}$-to-L_α transition. The compressed $L_{\beta'}$ phase in (*A*) under conditions of high pressure is characterized by tightly packed, all-*trans* acyl chains and a relatively large lamellar periodicity. Upon release of pressure, the $L_{\beta'}$ phase decompresses. This is accompanied by an increase in the cross-sectional area/acyl chain with the chains still adopting the rigid, all-*trans* configuration and by a decrease in the lamellar periodicity (*B*). The acyl chains then gradually disorder to form the L_α phase in (*C*). The decompression in the $L_{\beta'}$ phase (step 1: $A \rightarrow B$) is fast and is complete in 50 ms. The formation of the L_α phase from the decompressed $L_{\beta'}$ phase (step 2: $B \rightarrow C$) is the rate-limiting step requiring 1 s to complete.

(RI) to lower angles and 2) an increase in the scattering angle of the low-angle lamellar reflections. We believe that this same phenomenon is being observed in the course of the $L_{\beta'}$-to-L_α depressurization measurement series. Further, it accounts for the emergence of the "mysterious" RII reflection and the transient change in the low-angle reflection ob-

served immediately upon release of pressure on the $L_{\beta'}$ phase. Thus, upon formation of the uncompressed $L_{\beta'}$ phase, it begins to transform slowly to the L_α phase as water returns to the lipid in the rate-limiting step that effects full hydration of the new phase. Accordingly, in the current example, the depressurization jump is responded to by the compressed

hydrated lipid in the $L_{\beta'}$ phase in two discrete steps as follows.

$$\text{compressed } L_{\beta'} \quad \rightarrow \quad \text{uncompressed } L_{\beta'} \quad \rightarrow \quad L_\alpha.$$
$$\text{(RI)} \qquad \text{fast} \qquad \text{(RII)} \qquad \text{slow}$$

Upon first examining the wide-angle data in Fig. 4, we interpreted the progress curves as signaling the emergence of an intermediate in the $L_{\beta'}$-to-L_α phase transition. We were led to this conclusion in part because of the persistence of the RI reflection alongside the nascent L_α phase and the transient presence of the RII reflection. We ruled out the possibility of RII belonging to a transition intermediate by performing a depressurization jump within the compressed $L_{\beta'}$ phase (Fig. 6). Here, the RI reflection gave way to the RII reflection corresponding to the $L_{\beta'}$ phase at a reduced level of compression. As expected, the change was not accompanied by a phase transition. The fact that the peak position and area of the RII reflection stabilized with time after the depressurization jump suggests that a new equilibrium state has been achieved. This experiment serves to demonstrate convincingly that RII does not represent a heretofore unrecognized intermediate phase in the $L_{\beta'}$-to-L_α transition. Rather, it is a consequence simply of $L_{\beta'}$ phase decompression.

Certain of the wide-angle data recorded in live time during the depressurization jump experiment (see x-ray profile in Fig. 4 at 0.2 s) are reminiscent of that observed for the saturated phosphatidylcholines, e.g., dipalmitoylphosphatidylcholine (Tardieu et al., 1973), in the $L_{\beta'}$ phase. In the latter case, the scattering profile derives from a distorted hexagonal packing of the acyl chains (Tardieu et al., 1973). We do not consider this to account for the double-peaked feature in the current measurements for the following reasons. First, in separate equilibrium diffraction measurements on hydrated DHPE in the same temperature and pressure ranges covered in the dynamic experiments, a single symmetrical wide-angle peak was consistently observed (Cheng et al., manuscript in preparation). Secondly, in all depressurization jump experiments where RI and RII were sufficiently well resolved from one another, the area of the former but not of the latter peak decayed with a response profile similar to that of the detection/recording device. If RI and RII derived from the same underlying structure element they would be expected to respond in parallel.

The conversion from the compressed to the uncompressed $L_{\beta'}$ phase was at least as fast as the speed of the detection/recording system (Figs. 4, 5, and 6). There are two characteristics of lipid decompression within the $L_{\beta'}$ phase that may allow for such a fast response. The first concerns the limited and presumably rapid adjustment in the lipid configuration and molecular assembly that occurs during decompression in a single phase. This is in contrast to the large molecular rearrangements involved in the $L_{\beta'}$-to-L_α chain "melting" phase transition. The second characteristic is that decompression in the $L_{\beta'}$ phase probably involves little or no water movement and therefore is a "diffusionless" process. By comparison, the rate of the $L_{\beta'}$-to-L_α transition is possibly water diffusion-controlled given that, at atmospheric pressure at least, the L_α phase has four more water molecules associated with each lipid molecule than does the $L_{\beta'}$ phase (Hogan, 1989). In support of the former statement, we have found that the electron density profiles of hydrated DHPE in the $L_{\beta'}$ phase at various pressures and temperatures showed no significant change in the ratio of lipid layer thickness to lamellar repeat spacing (lipid-plus-water layer thickness) although the latter did vary with temperature and pressure (Cheng et al., manuscript in preparation). If we assume that the difference in the compressibility of lipid and water is negligible, a change in the lipid thickness-to-lamellar repeat ratio could indicate a change in the number of water molecules associated with the lipid. Our result therefore implies that little if any change occurs in the hydration properties of the $L_{\beta'}$ phase lipid upon release of pressure or a change in temperature. Without the need for water influx, the structure change associated with a simple decompression within the $L_{\beta'}$ phase is expected to be fast.

A similar two-step mechanism consisting of a structural relaxation within the original phase followed by the phase transition itself is to be expected in any large pressure or temperature jump perturbation measurement in which the initial condition places the sample in a given phase under conditions that are far removed from the transition involving that phase. When two discrete steps are not observed, several explanations are possible. Either the perturbation amplitude is not large enough or the spatial resolution of the detection/analysis method is not good enough to allow the limited structure relaxation to be seen. A short phase transition time can also limit the observability of the structure relaxation of the initial phase. In this case, both the original phase structure relaxation and the phase transformation may occur within the time resolution of the detector/analysis system. As a result, the only relaxation seen may be that associated with the equilibration of the nascent phase after the jump. Indeed, we suspect that this situation prevailed during the course of the pressurization jump experiments reported here. Since the L_α-to-$L_{\beta'}$ transition is fast for large amplitude pressure jumps (Table 1), the L_α phase underwent compression and converted to the $L_{\beta'}$ phase within the time resolution of the detection/recording system. This would account for our failure to observe compression of the L_α phase in any of the current measurements (Fig. 3). However, relaxation in the $L_{\beta'}$ phase after the transition over a period of 1–2 s was noted throughout the pressurization jump series (see peak position and height progress curves in Fig. 3). The latter is most likely related to the sample temperature reequilibrating after the transient adiabatic compression.

An in-phase structure relaxation that precedes the transition as described above was not observed in previous pressure jump studies of hydrated DHPE (Mencke and Caffrey, 1991). Of the low-angle diffraction that was monitored, only a continuous and smooth decrease in the lamellar repeat spacing was found in response to the pressure jump. We attribute this to the fact that a relatively high pressure is required for the gel phase to be compressed sufficiently to show any spatially resolved change upon decompression, especially in the

low-angle diffraction region. In support of this, we have found that in the current depressurization jump series neither a well developed RII peak nor a significant shift in the position of the low-angle reflection was observed in the lowest-amplitude pressure jump. Thus, the phenomenon would go unnoticed with any lower-amplitude pressure jump using DHPE and this TRXRD system as was the case in the previous work (Mencke and Caffrey, 1991).

To the best of our knowledge, the only other example of a two-step mechanism for a fast perturbation kinetic study of a lipid system involved a laser heating-induced L_α-to-inverted hexagonal (H_{II}) phase transition in fully hydrated 1-stearoyl-2-oleoyl-sn-glycero-3-phosphoethanolamine (SOPE) (Laggner and Kriechbaum, 1991; Laggner et al., 1989). This transformation occurs at about 57°C. In the latter study, the sample was first equilibrated at 50°C, and the transition was induced by a 10°C temperature-jump perturbation triggered by a 2- ms infrared laser pulse. The first step in the two-step response was described as involving a rapid decrease in the lamellar repeat spacing of the L_α phase to the extent of 3 Å. The slow transformation from the L_α to the H_{II} phase, representing the second step, was first noticeable 20 ms after the laser was fired. The proposed transition mechanism referred to an initial martensitic lattice disclination at a bilayer-normal plane which effected a reduction in the lamellar repeat spacing followed by the formation of a hexagonal lattice that grew out of the thin L_α phase so-formed (Laggner and Kriechbaum, 1991). In separate studies, we found that the lamellar repeat spacing of the L_α phase in hydrated DHPE can decrease by as much as 2 Å when temperature is raised by 10°C under equilibrium conditions (Caffrey, 1985; Cheng et al., 1992; Hogan, 1989). Accordingly, it is possible that the thinning of the lamellar structure observed in the first step of the transition involving SOPE above is a natural consequence of superheating the L_α phase effected by the 10°C temperature jump. As such, the thinning process may not be an integral part of the transition itself. It is of course reasonable to expect that the proper epitaxial relationship be established between the two interconverting phases for the transition to occur.

Limitations imposed by the time resolution of the detector/recording system

The difficulty in interpreting the two-step response of the $L_{\beta'}$ phase to depressurization arose primarily because of the limited time resolution of the detector/recording system coupled with a fast trigger and a rapidly responding system. A consequence of this is that the response of the sample within the $L_{\beta'}$ phase, for example, could not be monitored continuously in time and in parallel with the applied perturbation. This is in contrast to the situation in which the perturbation rate matches the time resolution of the detection/recording system as prevailed in the pressure-induced L_α-to-ripple phase transition in dimyristoylphosphatidylcholine (Caffrey et al., 1991). In this instance, the pressure jump from atmospheric pressure to 11.3 MPa

lasted ~1 s, and the response of the L_α phase to the "slowly" rising pressure could be followed easily and correlated with the latter. This serves to emphasize the need for making such kinetic measurements using instrumentation with suitable time resolution characteristics. Without this, interpretation of transition mechanisms based on kinetic measurements can prove difficult.

CONCLUSIONS

In this study, we have measured the $L_{\beta'}/L_\alpha$ transit time dependence on pressure jump amplitude for hydrated DHPE at 78°C in both the pressurization and depressurization directions. In the compression experiments, the chain disorder-to-order transit time decreased with increasing pressure jump amplitude and approached a limiting value of ~50 ms, which corresponds to the response time of the detection/recording system. Therefore, the intrinsic transit time for this barotropic phase change is ≤50 ms. The transit time for the depressurization jump-induced order-to-disorder transition did not show any dependence on pressure jump amplitude and consistently displayed a transit time of approximately 1 s. This value is considerably lower than what was reported previously where smaller pressure jump amplitudes and slower pressure jump speeds were used (Mencke and Caffrey, 1991).

The $L_{\beta'}/L_\alpha$ phase transitions of fully hydrated DHPE in the pressurization and depressurization directions were both found to be two-state to within the sensitivity limits of the system. Further, two steps were involved in the response of the $L_{\beta'}$ phase to the depressurization jump perturbation. The first involves a rapid structure rearrangement within the $L_{\beta'}$ phase in response to the large pressure and temperature drop caused by the adiabatic decompression. This is followed by the rate-limiting phase transformation. In contrast, a two-step response was not observed in the pressurization jump measurement primarily because the structural changes associated with the L_α-to-$L_{\beta'}$ transition are fast. Structure relaxation in the nascent $L_{\beta'}$ phase was observed and was driven by the thermal reequilibration of the sample after adiabatic compression.

This series of pressure jump measurements demonstrates the usefulness and the information-rich nature of the combined TRXRD and pressure jump technique in the study of lipid phase transitions. It also shows that the performance of the current detection/recording system is adequate for slower phase changes but may limit the intrinsic transit time measurements and mechanism interpretation in fast transitions.

REFERENCES

Caffrey, M. 1984. X-radiation damage of hydrated lecithin membranes detected by real-time x-ray diffraction using wiggler-enhanced synchrotron radiation as the ionizing radiation source. *Nucl. Instrum. Meth. Physics Res.* 222:329–338.

Caffrey, M. 1985. Kinetics and mechanism of the lamellar gel/lamellar liquid-crystal and lamellar/inverted hexagonal phase transition in phosphatidylethanolamine: a real-time x-ray diffraction study using synchrotron radiation. *Biochemistry.* 24:4826–4844.

Caffrey, M. 1987. Kinetics and mechanism of transitions involving the lamellar, cubic, inverted hexagonal and fluid isotropic phases of hydrated monoacylglycerides monitored by time-resolved x-ray diffraction. *Biochemistry.* 26:4826–4844.

Caffrey, M. 1989. The study of lipid phase transition kinetics by time-resolved x-ray diffraction. *Annu. Rev. Biophys. Biophys. Chem.* 18: 159–186.

Caffrey, M., J. Hogan, and A. Mencke. 1991. Kinetics of the barotropic ripple ($P_{\beta'}$)/lamellar liquid crystal (L_{α}) phase transition in fully hydrated dimyristoylphosphatidylcholine (DMPC) monitored by time-resolved x-ray diffraction. *Biophys. J.* 60:456–466.

Cheng, A., A. Minck, A. Mencke, J. Hogan, and M. Caffrey. 1992. The effect of pressure and temperature on the mesomorphism of hydrated DHPE examined by x-ray diffraction. *Biophys. J.* 61:A374.

Gruner, S. M. 1987. Time-resolved x-ray diffraction of biological materials. *Science.* 238:305–312.

Klug, H. P., and E. Alexander. 1974. X-Ray Diffraction Procedures. John Wiley and Sons, New York.

Laggner, P., and M. Kriechbaum. 1991. Phospholipid phase transitions: kinetics and structural mechanisms. *Chem. Phys. Lipids.* 57:121–145.

Laggner, P., M. Kriechbaum, A. Hernetter, F. Paltauf, J. Hendrix, and G. Rapp. 1989. Laser-induced temperature jump and time-resolved x-ray powder diffraction on phospholipid phase transitions. *Prog. Colloid Polym. Sci.* 79:33–37.

Marsh, D. 1991. General features of phospholipid phase transitions. *Chem. Phys. Lipids.* 57:109–120.

Mencke, A., A. Cheng, and M. Caffrey. 1993. A simple apparatus for time-resolved x-ray diffraction biostructure studies using static and oscillating pressures and pressure jumps. *Rev. Sci. Instrum.* 64:383–389.

Mencke, A. P., and M. Caffrey. 1991. Kinetics and mechanism of the pressure-induced lamellar order/disorder transition in phosphatidylethanolamine: a time-resolved x-ray diffraction study. *Biochemistry.* 30:2453–2463.

Seddon, J. M., G. Cevc, and D. Marsh. 1983. Calorimetric studies of the gel-fluid (L_{β}-L_{α}) and lamellar-inverted hexagonal (L_{α}-H_{II}) phase transitions in dialkyl- and diacylphosphatidylethanolamines. *Biochemistry.* 22:1280–1289.

Tardieu, A., V. Luzzati, and F. C. Reman. 1973. Structure and polymorphism of the hydrocarbon chains of lipids: a study of lecithin-water phases. *J. Mol. Biol.* 75:771–733.

Van Osdol, W. W., R. L. Biltonen, and M. L. Johnson. 1989. Measuring the kinetics of membrane phase transitions. *J. Biochem. Biophys. Methods.* 20:1–46.

Winter, R., C. L. Xie, J. Jonas, P. Thiyagarajan, and P. T. T. Wong. 1989. High-pressure small-angle neutron scattering (SANS) study of 1:2-dielaidoyl-sn-glycero-3-phosphocholine bilayers. *Biochim. Biophys. Acta.* 982:85–88.

Yager, P., and W. L. Peticolas. 1982. The kinetics of the main phase transition of aqueous dispersions of phospholipids induced by pressure jump and monitored by Raman spectroscopy. *Biochim. Biophys. Acta.* 668: 775–785.